frontiers | Frontiers in Earth Science

TYPE Original Research
PUBLISHED 02 June 2025
DOI 10.3389/feart.2025.1541337

OPEN ACCESS

EDITED BY
Ranjan Pramanik,
Indian Institute of Petroleum and Energy (IIPE), India

REVIEWED BY
Li Xianzhong,
Henan Polytechnic University, China
Zhongbei Li,
University of Wollongong, Australia

*CORRESPONDENCE
Zhongping Guo,
2042104161@qq.com

RECEIVED 07 December 2024
ACCEPTED 14 May 2025
PUBLISHED 02 June 2025

CITATION
Wang Z, Guo Z, Sun D, Zhang Y and Yang H (2025) Research on evolution law and mathematical model of pore fracture evolution in vertical slot coal under stress and gas relief.
Front. Earth Sci. 13:1541337.
doi: 10.3389/feart.2025.1541337

Research on evolution law and mathematical model of pore fracture evolution in vertical slot coal under stress and gas relief

Zhonghua Wang[1,2,3], Zhongping Guo[1]*, Dongling Sun[1,2,3], Yongjiang Zhang[2,3] and Huiming Yang[2,3]

[1]College of Energy and Mining Engineering, Shandong University of Science and Technology, Qingdao, China, [2]China Coal Technology Engineering Group Chongqing Research Institute, Chongqing, China, [3]State Key Laboratory of Coal Mine Disaster Prevention and Control, Chongqing, China

In order to solve the global problem of prevention and control of coal and gas outburst disaster dominated by ground stress in deep coal seam. It is found that hydraulic slotting and gas extraction have double pressure relief for coal seam horizontal stress and gas. The double pressure relief coefficient is proposed. Mechanical seepage experiments of coal samples with different double pressure relief coefficients (β = 0.5, 1.0, 1.5) were designed. The evolution mechanism and mathematical model of macro - fine - micro structure of coal seam fracture under the action of stress and gas relief are obtained. The results show that: with the increase of double pressure relief coefficient β, the fracture of vertical slot coal has a tendency to gradually weaken, and the fracture changes from tension failure to split failure, and from covering the whole coal body to the upper part of the coal. The macro-fracture plays a more dominant role than the micro fracture. When β = 1.0 ($\triangle\sigma$ = $\triangle P$), the macro fracture is the most developed. When β = 0.5 ($\triangle\sigma$ = 0.5$\triangle P$), the meso-fracture is the most developed. Before and after the test, the proportion of micropores and small pores is the largest, the proportion of large pores is the second, and the proportion of middle pores is the smallest. The proportion of cumulative fracture volume increased gradually and the growth rate was similar. It is found that there is a quadratic or cubic functional relationship between the fracture parameters of vertical slot coal under the double pressure relief coefficient β. It is found that there is a logarithmic function relationship between pore size and cumulative volume ratio. The research results provide a scientific basis for double pressure relief and permeability improvement of coal seam stress and gas, efficient extraction and effective outburst prevention.

KEYWORDS

vertical slot coal, coal and gas outburst, double pressure relief coefficient, pore fracture, evolution law, mathematical model

1 Introduction

Coal and gas outburst disasters, which are some of the most serious disasters in coal mines, frequently occur in coal mining (Yuan et al., 2023a; Yuan et al., 2023b; Pang, 2021; Shu, 2020; Xue S. et al., 2023; Guo et al., 2021). The prevention and control of coal and gas outbursts is a worldwide problem. For a long time, coal and gas outburst disasters have been very serious. For example, according to statistics, the cumulative number of accidents and deaths in China between 2013 and 2022 were 279 and 1,389, respectively. In addition, with the increase in coal mining intensity, coal resources have been gradually exhausted in shallow areas, and coal mines have been extended to deep mining worldwide (Yuan, 2021; Rong, 2020; Kang et al., 2023; Zhao and Zhang, 2020; Wei et al., 2022). A deep coal seam (more than 800 m) presents the characteristics of "three high and one low", such as high ground stress, high gas pressure, high gas content and low permeability (Qin et al., 2021; Hu, 2021; Yang, 2023; Chen et al., 2017; Agi et al., 2014; Zhang, 2020; Ren, 2022; Wang, 2022; Wang et al., 2012; Ying et al., 2020). The disaster-causing effect of ground stress on outbursts is more prominent. The dominant outburst type of ground stress occurs in deep coal seams after pre-pumping gas "up to standard" (Zhang et al., 2023; Zhao, 2022; Barbara, 2021; Yang et al., 2021). Therefore, it is urgent to explore the theoretical basis to prevent and control deep coal and gas outburst disasters dominated by stress.

Considering the difficulty of preventing and controlling deep stress-dominated outburst disasters, it is difficult to eliminate *in situ* stress hazards using only gas extraction. To this end, experts and scholars have studied and proposed spatial displacement pressure relief (including protective layer mining (Xue J. H. et al., 2023; Jia, 2022; Shi, 2023; Cheng et al., 2020; He et al., 2020; Tu and Cheng, 2019; Dang et al., 2021), pressure relief roadways (Li, 2019; Su et al., 2015), large-diameter drilling (Pang et al., 2021), hydraulic punching (Ren et al., 2022; Zhang et al., 2022; Zhang, 2021; Zhang et al., 2019), and hydraulic slotting (Zhang et al., 2018; Du, 2023; Yue, 2022; Zou et al., 2021; Cheng et al., 2021)) and coal and rock cracking pressure relief (hydraulic slotting, hydraulic fracturing (Wang and Li, 2022; Sun et al., 2017; Li, 2021; Zheng et al., 2023; Zhai et al., 2021; Li et al., 2021), CO_2 fracturing (Fan, 2021; Fan et al., 2021; Su, 2022), high-pressure air blasting (Li, 2023), etc.). The core scientific problem of these two pressure relief methods is to reform the structure of the coal rock mass and weaken its bearing characteristics to achieve stress transfer and pressure relief control. In general, the space displacement pressure relief mode has the disadvantages of a large engineering amount, a small pressure relief range and a low pressure relief efficiency, whereas the coal and rock cracking pressure relief mode has the advantages of a small engineering amount, a large pressure relief range and a high pressure relief efficiency. Hydraulic slotting technology can uniformly discharge a large quantity of coal chips in a coal seam, increase the expansion and deformation of the coal seam, and have a protective effect on layer mining. The stress state of the coal seam is effectively reduced, the extraction effect is improved, and the implementation is flexible. In addition, the combination of hydraulic seam cutting and gas extraction results in the double pressure relief of the ground stress and gas pressure of the coal seam, which has a marked effect on the prevention and control of deep ground stress-dominant outbursts and changes the pore fracture structural characteristics of the deep seam and slot coal.

Therefore, it is of great theoretical significance and practical value to study the macro-fine-micro-structure evolution law of coal seam pore fracture after coal seam hydraulic cutting, gas pumping and coal roadway driving until coal seam failure, and build a mathematical model.

At present, in terms of the macro-fine-micro-structure characteristics of pore fracture in fractured coal, Liu et al. (2015) proposed the organic combination of the liquid nitrogen adsorption method and mercury injection method to characterize the pore structure of coal after hydraulic slotting and gas pre-extraction and concluded that the synergistic effect of hydraulic slotting and gas extraction could weaken the gas adsorption capacity of coal and significantly improve the gas seepage capacity. Zou Q. L. et al. (2014), Zou Q. et al. (2014) used mercury injection experiments and low-temperature liquid nitrogen adsorption experiments to analyze the changes in coal gas adsorption characteristics after hydraulic slotting and gas pre-extraction and characterized the changes in pore size distribution and specific surface area of coal samples. However, the evolution law and mathematical model of the pore fracture structure of coal seam under the stress and gas relief have not been studied.

The vertical slot formed by hydraulic seams can relieve the horizontal stress, and gas extraction can relieve the gas pressure. Based on this well-known engineering background, the double pressure relief coefficient β is proposed in this paper. β is the ratio of the stress confining pressure reduction value $\triangle\sigma$ to the gas pressure reduction value $\triangle P$, i.e., $\beta = \triangle\sigma/\triangle P$. The hydraulic slit, gas extraction, coal roadway driving and outburst disaster evolution experiments were designed as mechanical seepage experiments of vertically fractured coal samples under different stress paths with double pressure relief coefficients. The macro-fine-micro evolution law of pore fracture before and after the test was studied, and a mathematical model was constructed. The results revealed the macro-micro mechanism of double pressure relief and permeability improvement of coal seam stress and gas, efficient extraction and effective outburst prevention. This study aims to provide a reference for the prevention theory and engineering application of deep coal and gas outburst disasters dominated by stress.

2 Materials and methods

2.1 Experimental background

2.1.1 Proposal of the double pressure relief coefficient

Figure 1 shows the diagram of double pressure relief of coal seam. The vertical slot formed by hydraulic cutting reduces the horizontal stress of coal seam. Borehole gas extraction reduces the gas pressure of coal seam. That is, hydraulic slotting + gas extraction reduces the stress and gas pressure of coal seam, which is called double pressure relief. For the quantitative study of double pressure relief, the ratio of horizontal stress (confining pressure) reduction $\triangle\sigma$ to gas pressure reduction $\triangle P$ is proposed as the double pressure relief coefficient, denoted as β. The formula is $\beta = \triangle\sigma/\triangle P$. The double pressure relief coefficient is the key parameter of the evolution law and mathematical model of macro - fine - micro pore fracture of vertical slot coal.

2.1.2 Engineering background

Before coal roadway is driven, it is necessary to adopt hydraulic slotting and gas extraction standard before coal roadway can be driven. In the process of coal roadway driving, the front coal seam

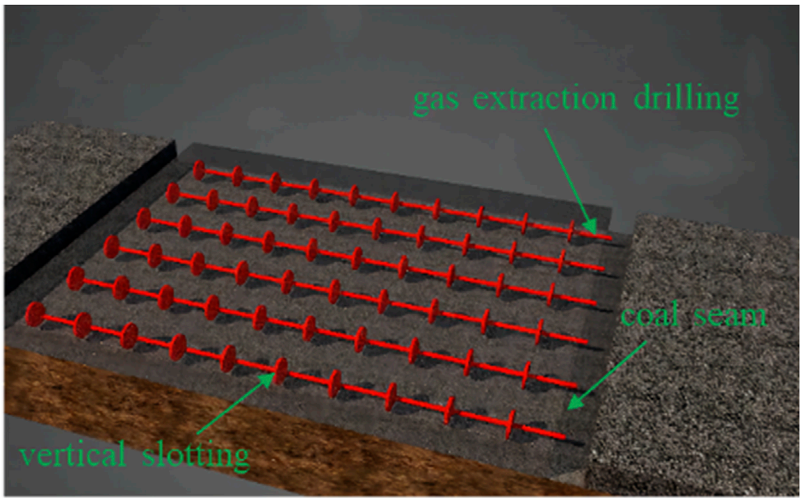

FIGURE 1
Schematic diagram of the double pressure relief of a coal seam.

will experience cyclic loading and unloading of stress. When the stress loading value exceeds the strength of coal seam, coal and gas outburst will occur. This is the engineering background for the later experiment.

2.2 Experimental scheme

2.2.1 Experimental procedure

Figure 2 shows the experimental process, which is mainly divided into four steps. As follows.

(1) Prepare vertical slot coal sample. Figure 2a is the physical diagram of vertical slot coal sample. In the standard coal sample, two slots with the size of 10 mm*10 mm*1 mm are prefabricated. The coal sample and slot size are made according to 1/20 of the actual project. Assuming that the thickness of the actual coal seam is 2 m and the seam groove is 2 cm, then the height of the coal sample is 100 mm and the height of the fracture is 1 mm. The cylinder coal samples are all drilled from the same large coal block of 0.5 m*0.5 m*0.5 m. In addition, the coal samples with vertical fractures were tested by ultrasonic longitudinal and horizontal wave automatic tester before and after production. The coal samples with large longitudinal wave velocity dispersion were excluded and the coal samples with similar wave velocity were selected to avoid the influence of the uneven coal samples on the test results.

(2) Mechanical seepage experiment. According to the engineering background in Section 2.1.2, mechanical seepage experiments were performed during hydraulic slotting, gas extraction and coal roadway driving of vertical-fracture coal samples. The experimental instrument was an RLW-500G coal-rock triaxial creep and seepage test system (Figure 2b).

(3) Macro-micro fracture structure test. A Phoenix v|tome| s industrial micro-CT scanning system (Figure 2c) was used to test the macro-micro fracture structure of the vertical slot coal before and after the test.

(4) Micropore structure test. A MesoMR12-150H-I nuclear magnetic resonance tester (Figure 2d) was used to test the microscopic pore structure of the vertical slot seam coal before and after the test.

Figure 3 shows the structure diagram of coal sample with vertical fracture.

2.2.2 Mechanical seepage experiment

2.2.2.1 Stress path

The engineering background of Section 2.1.2 is abstracted as the mechanical seepage experiment of a vertical-fracture coal sample under stress paths with different double pressure relief coefficients. The experimental process involves four stages: loading to the initial value (original rock stress); double pressure relief (hydraulic slit + gas extraction); cyclic loading and unloading (coal roadway driving); loading failure and post-peak loading (disaster evolution). The stress path of each stage is set as follows.

1) Primary rock stress: The vertical stress of the deep coal seam was set to σ_1 = 12 MPa, the horizontal stress was set to $\sigma_2 = \sigma_3$ = 8 MPa, and the gas pressure was set to P = 3.5 MPa.
2) Double pressure relief: Because vertical slots are formed in the coal seam after hydraulic slicing, vertical slots were prefabricated in the coal sample to simulate hydraulic slicing. When the gas pressure of the coal seam decreased after gas extraction, the gas pressure was set to decrease from the initial 3.5 MPa–0.5 MPa to simulate gas extraction.
3) Coal roadway driving: Because the coal roadway is always excavated, the coal body in front of the coal roadway produces a pre-stress concentration, and the stress concentration propagates forward in the form of stress waves. The coal body in front of the coal roadway experiences the effects of multiple stress concentration waves, each of which includes a period of

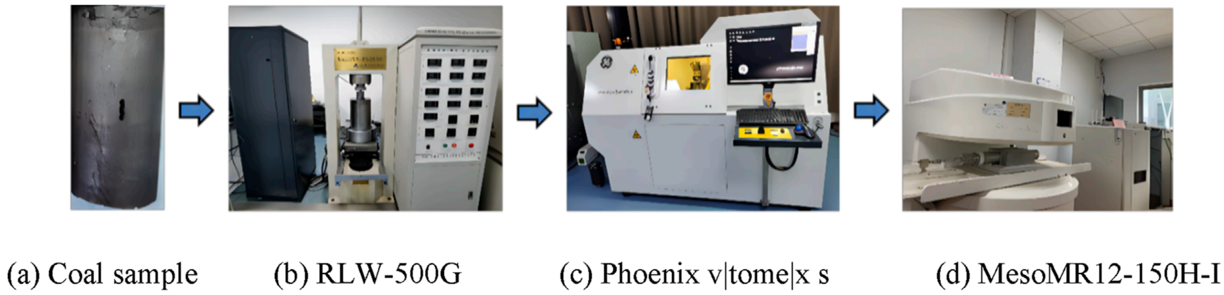

FIGURE 2
Experimental flow chart. **(a)** Coal sample **(b)** RLW-500G **(c)** Phoenix v|tome|x s **(d)** MesoMR12-150H-I.

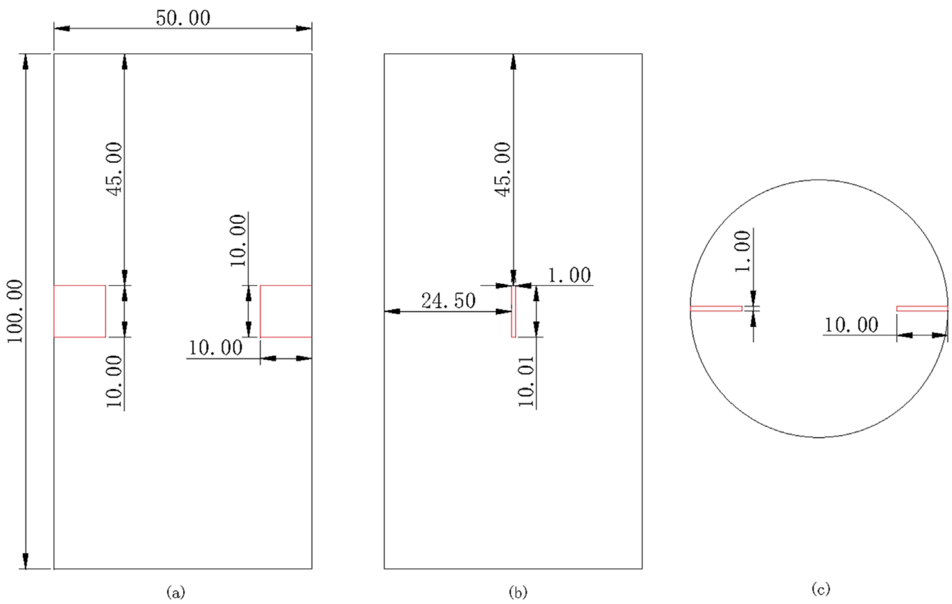

FIGURE 3
Structural diagram of a coal sample with a vertical fracture. **(a)** Mini View **(b)** left view **(c)** top view.

stress concentration loading and a period of pressure relief. Therefore, cyclic stress loading and unloading are used to simulate the influence of coal driving on the coal body.

4) Disaster evolution: If the disaster stress (energy) load exceeds the strength of the coal seam during coal roadway driving, the coal seam will be damaged and unstable, and outburst disasters occur. Therefore, the loading to coal body failure and post-peak loading to coal body instability are used to simulate the disaster evolution process.

2.2.2.2 Test process

Table 1 shows the stress paths in the four stages of the mechanical seepage test of the vertical slot coal sample. The loading rate in the initial loading phase was 0.01 MPa/s. In the double pressure relief stage, the confining pressure and gas pressure were simultaneously and evenly relieved, and the double pressure relief coefficient β was 0.5, 1.0, 1.5. The loading and unloading rates in the cyclic loading and unloading stage were 0.05 kN/s, 0.1 kN/s and 0.2 kN/s, and each loading and unloading rate occurred three times. After failure, the displacement loading rate was 0.1 mm/min until it became unstable. σ_1 is the vertical stress and $\sigma_2 = \sigma_3$ is the horizontal pressure.

Figure 4 shows the stress process of the mechanical seepage experiment of the vertical slot coal.

2.2.3 Macro-micro fracture structure test

Figure 5 shows the testing process of the macro-micro fracture structure, which includes two steps: CT scanning and 3D reconstruction.

1) Figure 5a shows the CT scanning process of a coal sample.

The coal samples before and after the test were placed between the X-ray tube and the detector. The X-ray emitted by the X-ray source passes through the coal sample, and the intensity of the X-ray is attenuated during the process. The attenuated X-ray illuminates the receiver, and the signal is automatically captured and stored by the image acquisition software. The test completes after a 360° rotation of the sample. The accuracy is 0.5 μm and the pixels is 30 frames.

TABLE 1 Test stress path (Unit: MPa).

Experimental phase	Experimental parameter	Loading and unloading rate
Load to the initial value	σ_1 = 12, σ_2 = σ_3 = 8, P = 3.5	0.01 MPa/s
Dual pressure relief (hydraulic slotting and gas extraction)	σ_1 = 12, σ_2 = σ_3 = 8–6.5, 8–5, 8–3.5, P = 3.5–0.5	β = 0.5, 1.0, 1.5
Cyclic loading and unloading (Coal driving)	σ_1 = 12–18	0.05 kN/s, 0.1 kN/s, 0.2 kN/s
Load failure and post peak loading (hazard evolution)	Load to failure, displacement load to instability	0.1 mm/min

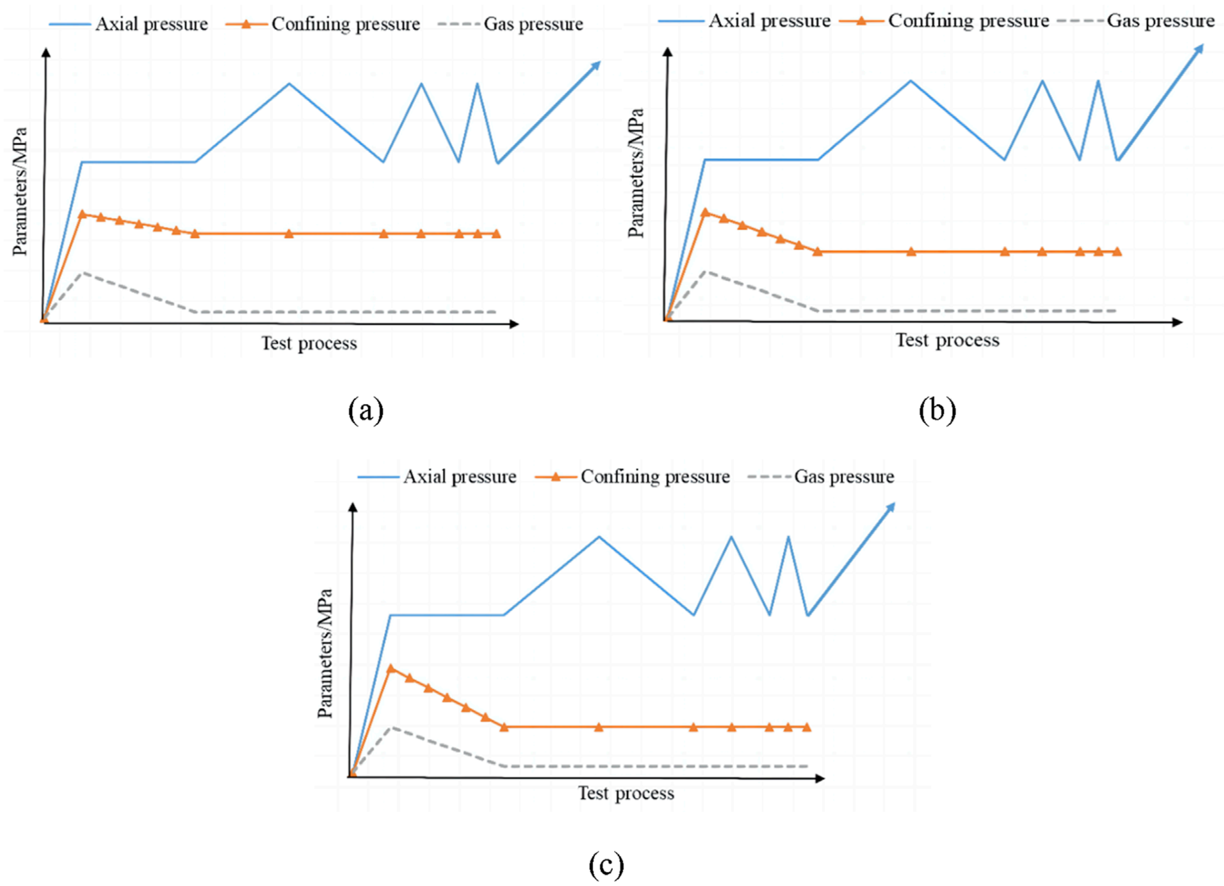

FIGURE 4
Test process (different double pressure relief coefficients β). **(a)** β = 0.5 **(b)** β = 1.0 **(c)** β = 1.5.

2) Figure 5b shows the three-dimensional reconstruction process of the coal sample.

CT scan data to be reconstructed are opened using the CT data reconstruction software phoenixdatos|x2, and the two-dimensional CT image data obtained from the CT scan are reconstructed into a three-dimensional structure.

2.2.4 Micropore structure test

2.2.4.1 Test Step

The micropore structure test includes three steps: sample preparation, test parameter setting, and porosity and aperture test calculation.

1) Sample preparation. First, the surface of the sample was cleaned of marl. Then, the sample was vacuumed with saturated deionized water at −0.1 MPa for approximately 10 h. Finally, the saturated sample was removed, free water on the sample surface was wiped with a wet paper towel, and the sample was wrapped in a nuclear magnetic coil using Teflon tape for testing.
2) Setting of test parameters. For the T_2 test, the CPMG sequence parameters were as follows: P_1 = 17.52 us, P_2 = 3.04 us, SW = 250 kHz, RFD = 0.08 ms, RG_1 = 20, DRG_1 = 2, PRG = 1, TW = 4,000 ms, TE = 0.15 ms, $NECH$ = 15,000, and NS = 16.
3) Measurement and calculation of the porosity and aperture. The coal sample data were obtained using the CPMG sequence

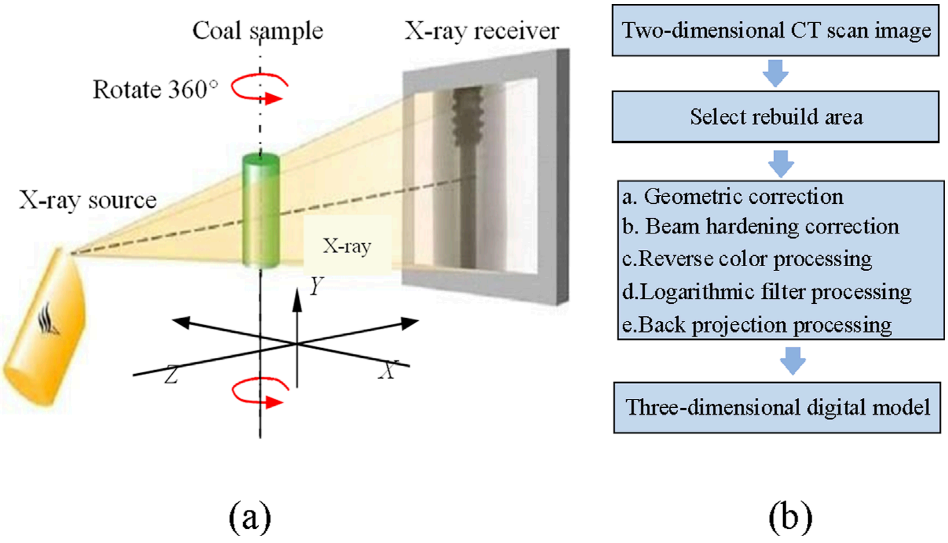

FIGURE 5
Test flow of the macro-micro fracture structure of the coal sample. **(a)** CT scan **(b)** 3D reconstruction.

in the nuclear magnetic resonance analysis software. The porosity standard sample was calibrated, and the porosity of the sample was obtained *via* calculations. The sample T_2 spectra were obtained by inverting the sampled data using an inversion software.

2.2.4.2 Porosity

For the nuclear magnetic signal measured by the coal sample with saturated water, the standard scale sample was used for calibration, the signal strength was converted into the porosity as follows (Han, 2022):

$$\varphi = \Phi * \frac{s}{S} * \frac{NS}{ns} * 10^{\frac{1}{20}(RG1-rg1)} * 2^{(RG2-rg2)} \tag{1}$$

In Formula 1, Φ is the porosity of the standard sample, φ is the porosity of the sample to be tested, *NS* is the accumulation time of the standard sample, *ns* is the accumulation time of the sample to be tested, *S* is the nuclear magnetic signal value of the standard sample, and *s* is the nuclear magnetic signal value of the sample to be tested.

2.2.4.3 Aperture distribution

The T_2 spectrum of the sample is obtained by using the SIRT inversion algorithm for mathematical inversion of the echo attenuation signal collected from the sample. There are three different relaxation mechanisms for fluids in pores: free relaxation, surface relaxation, and diffusion relaxation, which can be expressed as follows (Kenyon, 1992):

$$\frac{1}{T_2} = \frac{1}{T_{2S}} + \frac{1}{T_{2B}} + \frac{1}{T_{2D}} \tag{2}$$

In Formula 2, T_2 is the transverse relaxation time of the pore fluid collected through the CPMG sequence; T_{2s} is the transverse relaxation time of the pore fluid in a sufficiently large container (so large that the container effect is negligible); T_{2B} is the transverse relaxation time caused by surface relaxation; T_{2D} is the transverse relaxation time caused by diffusion under a magnetic field gradient.

When a short TE is used and the pores contain only water, surface relaxation plays a major role; i.e., T_2 is directly proportional to the pore size (Kleinberg et al., 1994):

$$\frac{1}{T_2} \approx \frac{1}{T_{2S}} = \rho_2\left(\frac{S}{V}\right) \tag{3}$$

In Formula 3, ρ_2 is the surface relaxation rate, and $\left(\frac{S}{V}\right)$ is the specific surface area of the pore.

For pore structure test samples that can be simplified into spherical pores and columnar pipes, the above formula can be further simplified into the relationship between T_2 relaxation time and coal core pore radius r_c, i.e., (Yao and Liu, 2016):

$$\frac{1}{T_2} = F_s\left(\frac{\rho_2}{r_c}\right) \tag{4}$$

In Formula 4, F_s is the geometric shape factor (spherical pores: $Fs = 3$; columnar pores: $F_s = 2$).

Therefore, the T_2 distribution map reflects the pore size distribution: small pores have small T_2; large pores have large T_2.

Assuming that a pore is a cylinder with radius *r*, the calculation assumes that the coal core velocity is 50 μm/s, so it can be converted to a pore size distribution map. Based on Equations 3 and 4, the transverse surface relaxation rate ρ_2 is obtained using this method. However, ρ_2 cannot be directly calculated, and it is often necessary to indirectly obtain the value by combining it with a nitrogen adsorption curve or a mercury injection curve. In this experiment, the mercury injection curve was used to indirectly obtain the value.

3 Pore fracture characteristics

According to the experimental results, fractures larger than 1 mm are classified as macroscopic fractures, fractures between 1 mm and 1 μm are classified as microscopic fractures, and fractures smaller than 1 μm are classified as microscopic pores. The pore fracture characteristics are obtained, which are described as follows.

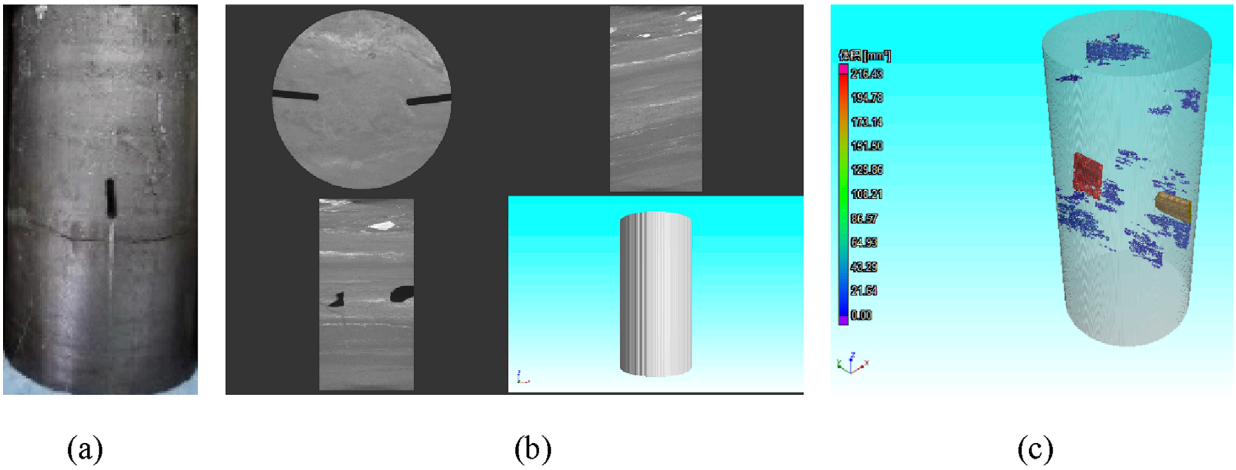

FIGURE 6
Vertical-fracture coal sample (before test). **(a)** Physical image **(b)** CT scan image **(c)** Three-dimensional pore and fracture re-composition.

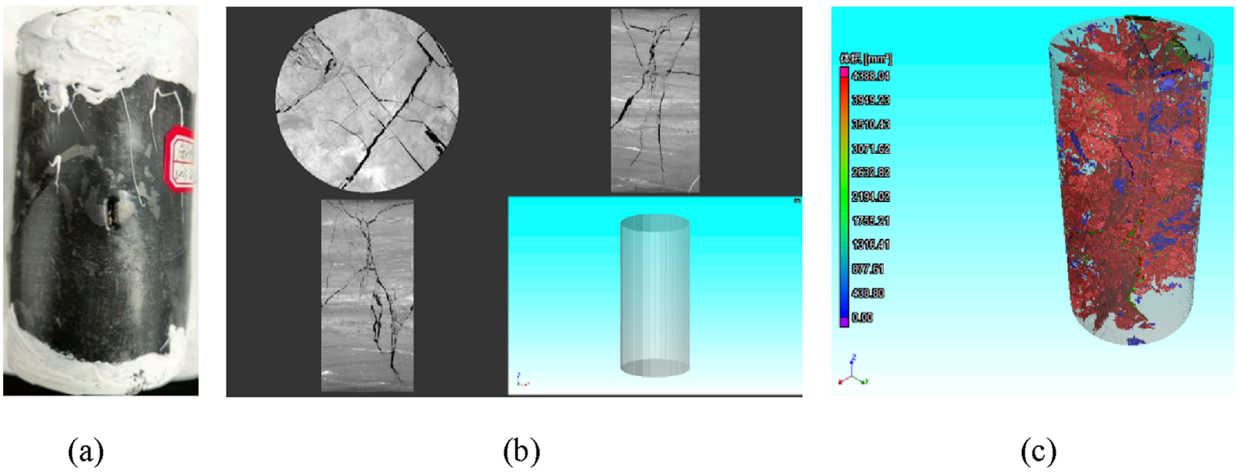

FIGURE 7
Failure pattern of the vertical-fracture coal sample after the test (β = 0.5). **(a)** Physical image **(b)** CT scan image **(c)** Three-dimensional pore and fracture re-composition.

3.1 Macro-micro fracture

Figure 6 shows the physical map, three views of CT scan and three-dimensional recomposition of the vertical slot coal sample before the test (the shape of the three coal samples is basically the same, taking β = 1.0 as an example). Figures 7–9 show the physical diagram, CT scan view and three-dimensional fracture re-composition of vertical slot coal sample after the double pressure relief coefficient β = 0.5, 1.0 and 1.5 tests, respectively. The top left image is the top view, the top right image is the right view, the bottom left image is the main view, and the bottom right image is the three-dimensional digital model. The fracture development law, type and regional distribution law of vertical slot coal sample are obtained, detailed as follows.

3.1.1 Fracture development law

Figure 6 shows that the vertical-fracture coal sample had no macroscopic fracture except the vertical fracture before the test. After the tests with double pressure relief coefficient β = 0.5, 1.0 and 1.5, Figures 7–9 show that the overall degree of fracture development gradually decreased in the top view, right view and main view of the two-dimensional CT scan. The degree of fracture development in the main view was greater than that in the right view with the same double pressure relief coefficient.

3.1.2 Classification of fracture types

After the tests with double pressure relief coefficient β = 0.5, 1.0, and 1.5, Figures 7–9 show that the main fracture types were tensile fracture, tensile fracture, and through-splitting

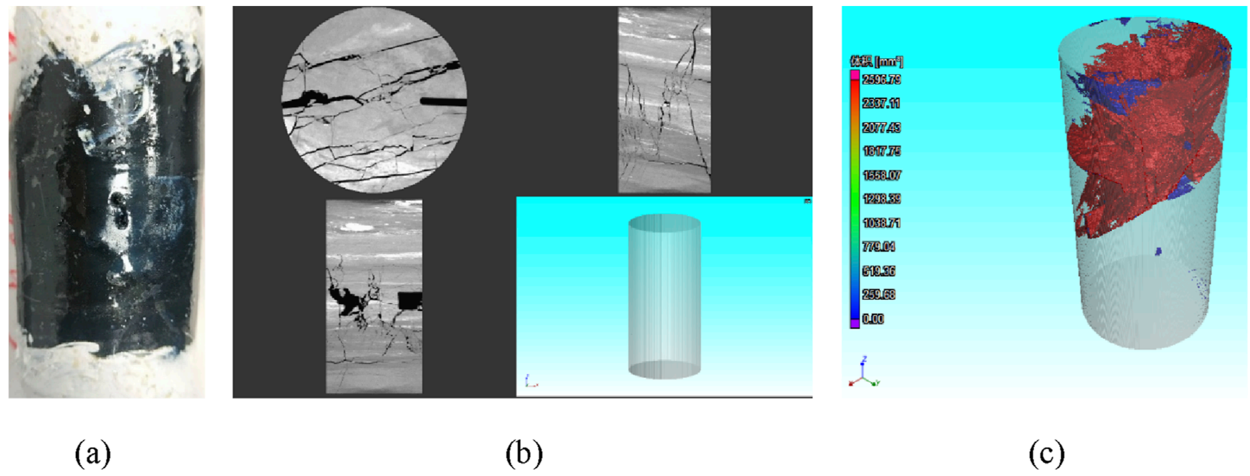

FIGURE 8
Failure pattern of the vertical-fracture coal sample after the test (β = 1.0). **(a)** Physical image **(b)** CT scan image **(c)** Three-dimensional pore and fracture re-composition.

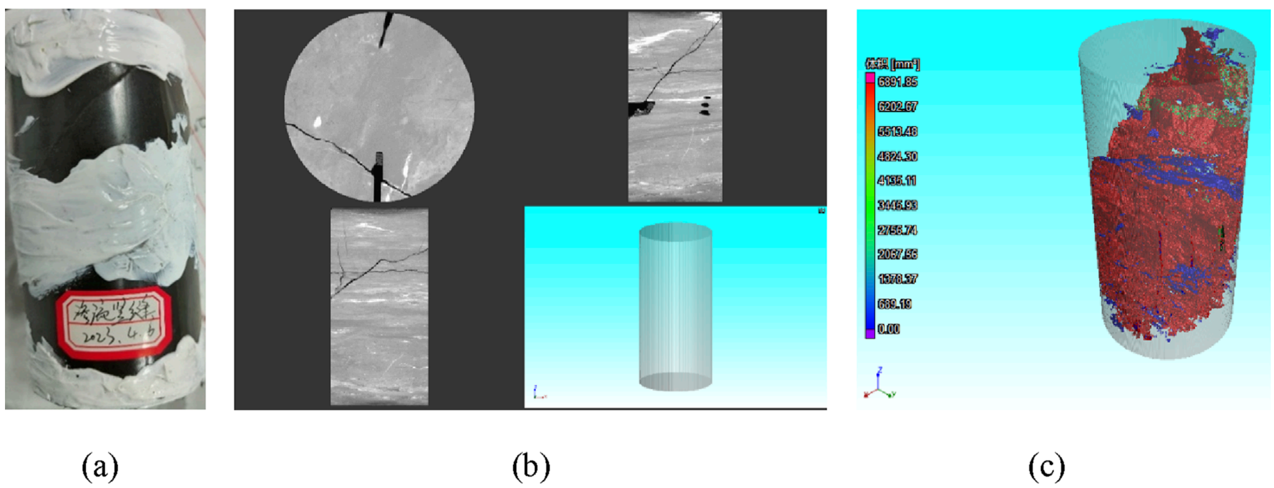

FIGURE 9
Failure pattern of the vertical-fracture coal sample after the test (β = 1.5). **(a)** Physical image **(b)** CT scan image **(c)** Three-dimensional pore and fracture re-composition.

fracture, respectively, in the top view, right view, and main view of the two-dimensional CT scan of the vertical-fracture coal sample. However, there were differences in the fracture angle and splitting angle. The degree of fracture development gradually decreased.

3.1.3 Regional distribution of fracture

After the tests with double pressure relief coefficient β = 0.5, 1.0 and 1.5, Figures 7–9 show that the main fracture areas were 2.5–7.5 cm from the lower end face, 2.5–7.5 cm from the lower end face, and the upper part in the top view of the two-dimensional CT scan of the vertical-fracture coal sample. The right view and the main view show that the main fracture areas were the entire coal body, entire coal body and upper part, but there were differences in the degree of fracture development.

The above experimental results can provide theoretical basis for the space design, prediction and control of fractures.

3.2 Microscopic pores

Figure 10 shows the T_2 spectra and pore parameters before the vertical slot coal sample test and after the double pressure relief coefficient β = 0.5, 1.0 and 1.5 tests. According to the peak division method, the first peak of the T_2 spectrum from left to right corresponds to mesopores, the second peak corresponds to mesopores, and the third peak corresponds to macropores and fractures. According to Hodot method, the porosity can be divided into micropores (<0.01 microns), mesopores (0.01–1 micron) and macropores (>1 micron) (Zhai et al., 2022).

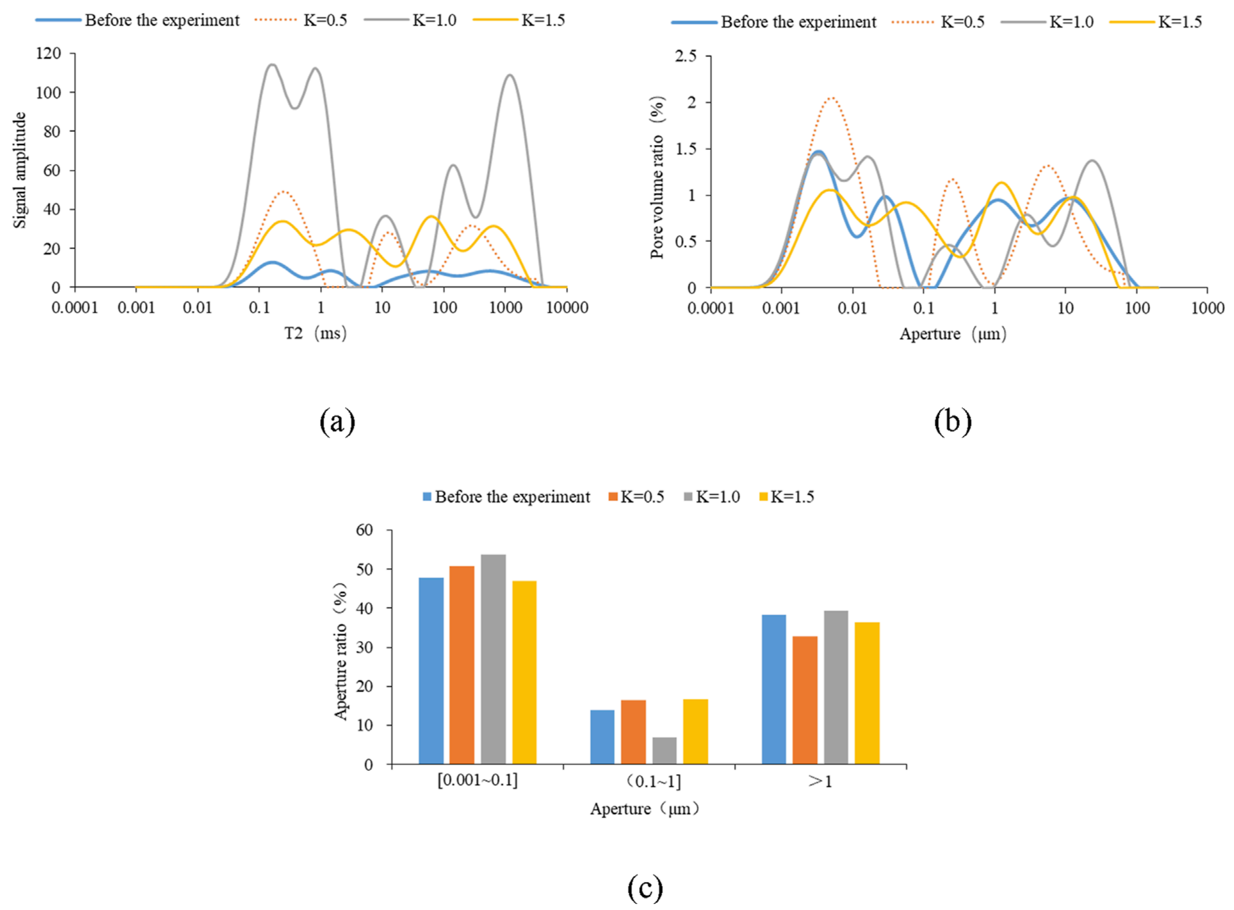

FIGURE 10
T_2 spectra and pore parameters before and after the test. **(a)** T_2 spectrum **(b)** Pore volume ratio of different pore sizes **(c)** Histogram of pore radius distribution.

3.2.1 T_2 spectral characteristics

Figure 10a shows that the signal intensity of the vertical slot coal sample before the test has four relatively uniform peaks. After the tests with double pressure relief coefficient β = 0.5, 1.0 and 1.5, the pore volume ratio of the vertical slot coal sample had three, five and four peaks, respectively, which were also relatively uniform.

3.2.2 Pore volume ratio of different pore sizes

Figure 10b shows that the pore volume ratio of the vertical slot coal sample has four peaks before the test, which are relatively uniform. The results show that pore micropores, mesopores and fractures were evenly distributed before the test. After the tests with double pressure relief coefficient β = 0.5, 1.0 and 1.5, there were three, five and four peaks, respectively, for the pore volume ratio of the vertical slot coal sample. In descending order, the peak values are for double pressure relief coefficients β = 0.5, 1.0, and 1.5. The comparative analysis shows that the pore size of the same aperture is larger after the test than before the test.

3.2.3 Pore radius distribution rule

In Figure 10c, the volume proportions of the cumulative pore sizes are different; the proportion of micropores and mesopores was in the order of β = 0.5, β = 1.0, β = 1.5 and before the test with 53.70%, 50.73%, 47.83% and 46.96%, respectively. Thus, the proportion of micropores and mesopores increases before the comparison test when $\triangle\sigma \leq \triangle P$. The proportion of micropores and mesopores decreases when $\triangle\sigma > \triangle P$. In descending order, the proportion of mesopores was β = 1.5, β = 1.0, before the test, and β = 0.5 with 16.65%, 16.52%, 13.97% and 6.86%, respectively. Thus, the proportion of mesopores decreases before the comparison test when $\triangle\sigma = \triangle P$. The proportion of mesopores increases compared with that before the test when $\triangle\sigma \neq \triangle P$. The proportion of macropores was 39.43%, 38.20%, 36.39% and 32.75% for β = 0.5, β = 1.5, before the test, and β = 1.0, respectively. Thus, the macropore ratio increases before the comparison test when $\triangle\sigma = \triangle P$. The proportion of macropores decreases before the test when $\triangle\sigma \neq \triangle P$.

Comparatively, before the test, micropores and mesopores had the largest proportion (47.83%), followed by the proportion of macropores (38.20%), and mesopores had the smallest proportion (13.97%). After the tests with double pressure relief coefficient β = 0.5, 1.0, and 1.5, the order remained: micropores and mesopores had the largest proportion (46.96%–53.70%), macropores had the second largest proportion (32.75%–39.43%), and mesopores had the smallest proportion (6.86%–16.65%). Thus, micropores and mesopores have the largest proportion before and after the

TABLE 2 Macro fracture parameters before and after the test.

Fracture parameter	Before test	After test		
		β = 0.5	β = 1.0	β = 1.5
Radius (mm)	154.19	449.64	431.13	129.22
Volume (mm^3)	481.12	202.23	7140.33	2790.24
Surface area (mm^2)	3599.11	5532.59	86,036.43	38,023.1

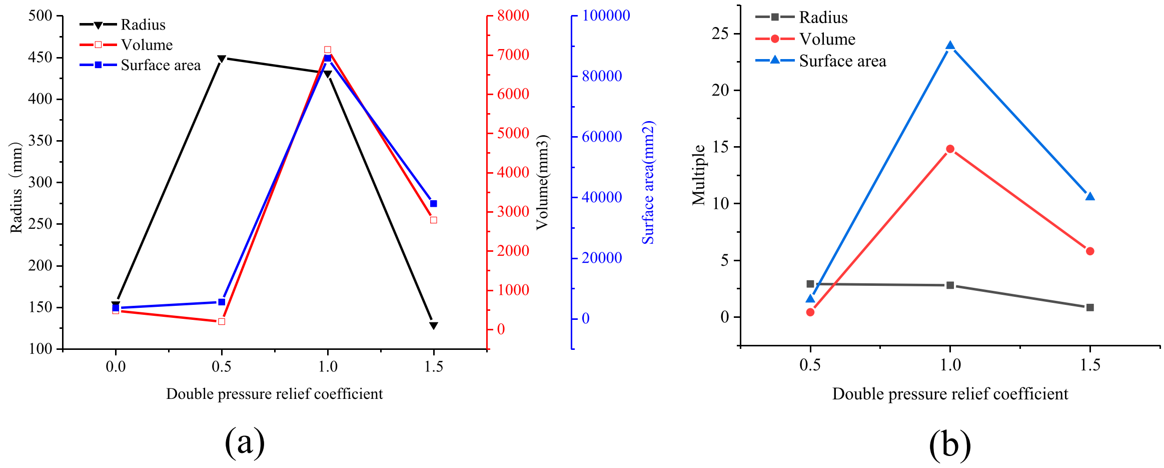

FIGURE 11
Variation law of the macro fracture parameters. **(a)** Parameter **(b)** Multiple.

test, followed by macropores, and mesopores have the smallest proportion.

4 Evolution law and mathematical models

According to the test results, the evolution law of pore fracture parameters under double pressure relief was studied, and a mathematical model was established, detailed as follows.

4.1 Macroscopic fracture

4.1.1 Evolution law

Table 2 shows the macroscopic fracture parameters before and after the test of double pressure relief coefficient β = 0.5, 1.0 and 1.5 for vertical slot coal samples. Figure 11a shows the change curve of macroscopic fracture radius, volume and surface area. Figure 11b shows the multiples of macroscopic fracture radius, volume and surface area after the test compared with that before the test.

As shown in Figure 11a, before and after the vertical-fracture coal sample test, the cumulative radius of the macroscopic fractures followed the order of β = 0.5, β = 1.0, before the test, and β = 1.5. The descending order for the cumulative macro fracture volume and surface area was β = 1.0, β = 1.5, β = 0.5, and before the test. When $\triangle\sigma \le \triangle P$, the macro fracture radius was larger than that before the test. When $\triangle\sigma > \triangle P$, the macro fracture radius was smaller than that before the test. When $\triangle\sigma \ge \triangle P$, the macro fracture volume and surface area were larger than those before the test. When $\triangle\sigma < \triangle P$, the macro fracture volume and surface area decreased.

Figure 11b shows that the radius, volume, and surface area of the macro fractures decrease in the order of β = 1.0, β = 0.5, β = 1.5, and after the tests. The macro fracture radius increased by 2.92 times, 2.80 times and 0.84 times, respectively. The macro fracture volume increased by 0.42 times, 14.83 times and 5.80 times, respectively. The macro fracture surface area increased by 1.54 times, 23.90 times and 10.56 times, respectively. Thus, macro fractures are the most developed with double pressure relief coefficient β = 1.0 ($\triangle\sigma = \triangle P$).

The research results can provide theoretical basis for scientific layout of macroscopic fractures in seam and reasonable determination of borehole spacing and sealing length of gas extraction.

4.1.2 Mathematical model

In order to better apply the research results to engineering practice, a numerical model of macro-fractures surface area, radius, volume with double pressure relief coefficient β under triaxial loading β = 0 and double pressure relief coefficient β = 0.5, 1.0 and 1.5 was constructed, as shown in Formula 5. For the numerical model

TABLE 3 Microfracture parameters before and after the test.

Fracture parameter	Before test	After test		
		β = 0.5	β = 1.0	β = 1.5
Radius (mm)	53.5	348.13	255.32	150.86
Volume (mm^3)	1.67	26.6	23.9	3.4
Surface area (mm^2)	77.38	905.14	715.13	164.2

of the surface area, radius and volume increase times of the macro-fractures with the double pressure relief coefficient β after double pressure relief, as shown in Formula 6.

$$\begin{cases} H_{\text{shb}} = -276117K^3 + 571316K^2 - 212762K + 3599.1 \\ H_{\text{shr}} = -24673K^3 + 51444K^2 - 20112K + 481 \quad\quad (0 \le \beta \le 1.5) \\ H_{\text{shv}} = 40.747K^3 - 689.04K^2 + 925.23K + 154.19 \end{cases} \tag{5}$$

$$\begin{cases} B_{\text{shb}} = -71.4K^2 + 151.82K - 56.52 \\ B_{\text{shr}} = -46.88K^2 + 99.14K - 37.43 \quad (0.5 \le \beta \le 1.5) \\ B_{\text{shv}} = -3.68K^2 + 5.28K + 1.2 \end{cases} \tag{6}$$

In Formula 5 and 6, H_{shb}, H_{shr}, H_{shv} represent the surface area, radius and volume of macro-fractures in prefabricated vertical slot coal samples, respectively. B_{shb}, B_{shr}, B_{shv} is the increase times of surface area, radius and volume of macro-fractures after double pressure relief compared with that before the test, respectively.

The above mathematical model can quantitatively design, predict and control the macroscopic fracture spatial distribution of seam and groove seam, so as to improve the gas permeability, pumping effect and outburst prevention effect of coal seam.

4.2 Microscopic fracture

4.2.1 Evolution law

Table 3 shows the cumulative microfracture radius, volume and surface area before and after the tests with double pressure relief coefficient β = 0.5, 1.0 and 1.5 for the vertical-fracture coal samples. Figure 12a shows the cumulative size change curves of the radius, volume and surface area of the micro fracture before and after the test. Figure 12b shows the multiples of the radius, volume and surface area of the microfracture after the test compared with those before the test.

Figure 12a shows that after the test, the cumulative micro-fracture radius, volume and surface area of the vertical-fracture coal sample followed the decreasing order of β = 0.5, β = 1.0, and β = 1.5. In other words, with increasing double pressure relief coefficient, parameters such as the radius, volume and surface area of the microfracture gradually decrease.

As shown in Figure 12b, after the tests with double pressure relief coefficient β = 0.5, 1.0 and 1.5, when the double pressure relief coefficient increased, the increase in radius, volume and surface area of the microfracture gradually decreased. The microfracture radius was 6.51 times, 4.77 times and 2.82 times of that before the test; the microfracture volume was 15.99 times, 14.34 times and 2.04 times of that before the test; the microfracture surface area was 11.70 times, 9.24 times and 2.12 times of that before the test, respectively. Thus, the microfracture is most developed when the double pressure relief coefficient is β = 0.5 ($\triangle\sigma$ = 0.5$\triangle P$) for the vertical-fracture coal sample.

The experimental results can provide scientific basis for rational arrangement of meso-fracture network of seam.

4.2.2 Mathematical model

The numerical model of micro-fractures surface area, radius, volume with double pressure relief coefficient β under triaxial loading β = 0 and double pressure relief coefficient β = 0.5, 1.0 and 1.5 was constructed, as shown in Formula 7. For the numerical model of the surface area, radius and volume increase times of the micro-fractures with the double pressure relief coefficient β after double pressure relief, as shown in Formula 8.

$$\begin{cases} H_{\text{sxb}} = -1378.7K^2 + 2082.1K + 110.22 \\ H_{\text{sxr}} = -399.09K^2 + 638.49K + 72.289 \quad (0 \le \beta \le 1.5) \\ H_{\text{sxv}} = -45.43K^2 + 68.643K + 2.1615 \end{cases} \tag{7}$$

$$\begin{cases} B_{\text{sxb}} = -9.32K^2 + 9.06K + 9.5 \\ B_{\text{sxr}} = -0.42K^2 - 2.85K + 8.04 \quad (0.5 \le \beta \le 1.5) \\ B_{\text{sxv}} = -21.3K^2 + 28.65K + 6.99 \end{cases} \tag{8}$$

In Formula 7 and 8, H_{sxb}, H_{sxr}, H_{sxv} represent the surface area, radius and volume of micro-fractures in prefabricated vertical slot coal samples, respectively. B_{sxb}, B_{sxr}, B_{sxv} are the increase times of surface area, radius and volume of micro-fractures after double pressure relief compared with that before the test, respectively.

The above mathematical model can be used to quantitatively design, predict and control the spatial distribution of micro-fracture in seam, so as to improve the gas permeability, pumping effect and outburst prevention effect of coal seam.

4.3 Macro-microfracture

4.3.1 Evolution law

In order to obtain the magnitude of the leading role of macroscopic fracture and microscopic fracture on coal body, the multiples of fracture radius, volume and surface area before and after the macro-microscopic fracture test were calculated, and the number of macroscopic fracture and microscopic fracture were

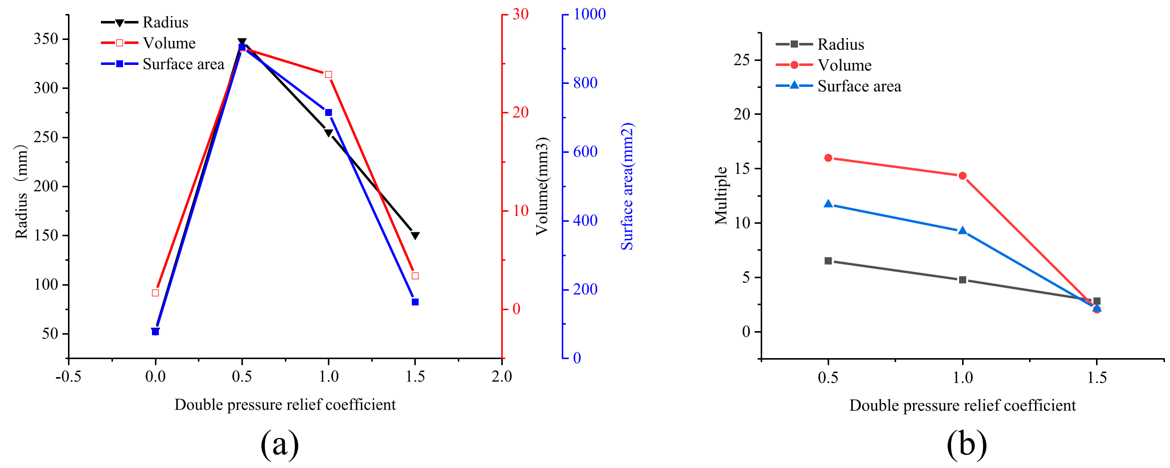

FIGURE 12
Change law of the microfracture parameters. **(a)** Parameter **(b)** Multiple.

TABLE 4 Macroscopic and microscopic fracture parameters before and after the test.

Fracture parameter	Before test	After test		
		β = 0.5	β = 1.0	β = 1.5
Radius	2.88	1.29	1.69	0.86
Volume	288.02	7.59	298.74	820.59
Surface area	46.51	6.11	120.31	231.57
Number of macro fracture	38	224	175	31
Number of micro fracture	561	2343	651	227

counted, as shown in Table 4. Figure 13a shows the change curve of the multiple relation. Figure 13b shows the change curve of fracture number.

The macro fractures had greater radius, volume and surface area than the microfractures, which indicates the dominant role of macro fractures. According to Table 4, the microfracture radius had the following descending order: before the test, β = 1.0, β = 0.5, and β = 1.5. In other words, the leading role of the macro fracture radius weakened after the double pressure relief. The dominant sizes of the volume and surface area of macro fractures followed the order of β = 1.5, β = 1.0, before the test, and β = 0.5. Thus, the dominant role of the volume and surface area of macro fractures decreased after the test when $\triangle\sigma<\triangle P$. The volume and surface area of macro fractures played a more dominant role after the test when $\triangle\sigma\geq\triangle P$.

Figure 13a shows that macro fractures had greater radius, volume, surface area than microfractures before and after the tests with β = 0.5, 1.0, and 1.5. The macro fracture was 0.86–2.88 times, 7.59–820.59 times and 6.11–231.57 times of the microfracture, respectively, i.e., macro fractures played a leading role.

Figure 13b shows that the number of macro- and micro-fractures follows the decreasing order of β = 0.5, β = 1.0, β = 1.5, and before the test, before and after the test with 224, 175, 38 and 31 macro fractures and 2343, 651, 561 and 227 microfractures, respectively. In other words, the number of macroscopic and microscopic fracture before the test was greater than that at β = 1.5 and less than those at β = 0.5 and β = 1.0. The results show that there were more macro-micro fractures after the test when $\triangle\sigma\leq\triangle P$. There were fewer macro-micro fractures after the test when $\triangle\sigma>\triangle P$.

It is calculated that the number of micro fractures before and β = 0.5, 1.0 and 1.5 are 14.76 times, 10.46 times, 3.72 times and 7.32 times of the number of macro fractures, respectively. It is concluded that with the increase of the double pressure relief coefficient, the number of macro fractures and the number of micro fractures decrease gradually, and the reduction rate of the number of micro fractures fracture is larger.

The experimental results provide theoretical basis for determining the effect of macroscopic fracture and microscopic fracture on the increase of gas permeability of seam.

4.3.2 Mathematical model

The numerical models of the multiples of the radius, volume and surface area of macro fractures and micro fractures with the double pressure relief coefficient β of prefabricated vertical slot coal samples are constructed, as shown in Formula 9. For the numerical model of

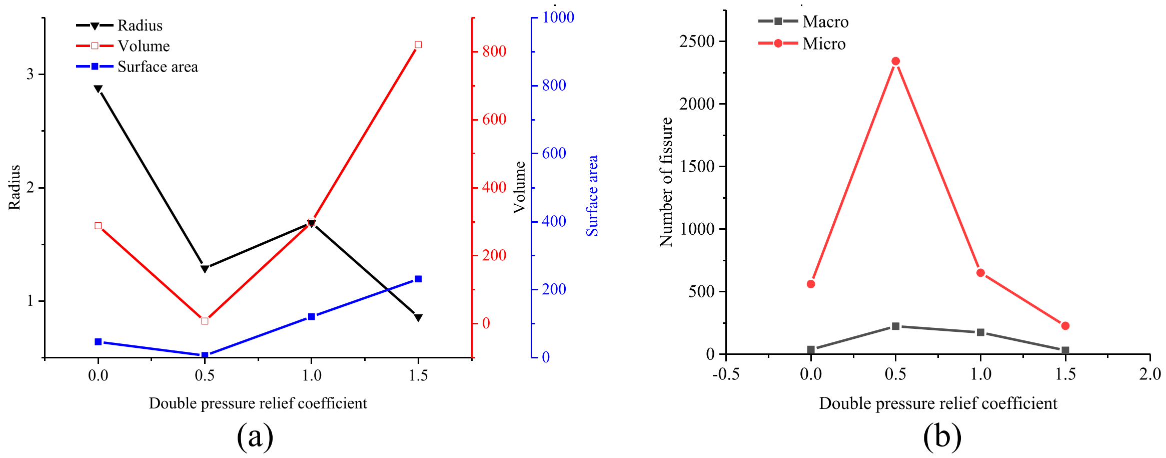

FIGURE 13
Comparison of the macro fracture and microfracture parameters. **(a)** Multiple fractures **(b)** Number of fractures.

the number of macro fractures, the number of micro fractures with the double pressure relief coefficient β of prefabricated vertical slot coal samples, as shown in Formula 10.

$$\begin{cases} B_{shxb} = 151.66K^2 - 93.614K + 38.633 \\ B_{shxr} = 0.76K^2 - 2.272K + 2.719 \\ B_{shxv} = 802.28K^2 - 825.65K + 270.98 \end{cases} \quad (0 \le \beta \le 1.5) \qquad (9)$$

$$\begin{cases} L_{sh} = 6322.7K^3 - 16432K^2 + 10199K + 561 \\ L_{sx} = -330K^2 + 481K + 45 \end{cases} \quad (0 \le \beta \le 1.5) \qquad (10)$$

In Formula 9 and 10, B_{shxb}, B_{shxr}, B_{shxv} are the multiples of the radius, volume and surface area of the macro-fractures and micro-fractures in the prefabricated vertical slot coal samples, respectively. L_{sh}, L_{sx} are the number of macro-fractures and the number of micro-fractures in the prefabricated vertical slot coal samples, respectively.

The above mathematical model can quantitatively determine the multiples of macroscopic fractures and microscopic fractures in seam and can also quantitatively design, predict and control the spatial network distribution of macroscopic fractures and microscopic fractures in seam, so as to improve the gas permeability, pumping effect and outburst prevention effect of coal seam.

4.4 Microscopic pores

4.4.1 Evolution law

Figure 14 shows the cumulative pore volume ratio of coal samples before vertical fracture test and after double pressure relief coefficient β = 0.5, 1.0 and 1.5. As can be seen from.

Figure 14, the cumulative pore volume ratio of vertical slot coal samples before the test and after β = 0.5, 1.0, and 1.5 tests basically began to increase from 0.01 μm. The cumulative pore volume ratio of different paths increases gradually, and the increasing speed is similar.

The experimental results reveal the increase of gas permeability, efficient extraction and effective outburst prevention mechanism of seam from the microscopic point of view.

4.4.2 Mathematical model

The mathematical model of different pore diameter and cumulative volume ratio of vertical slot coal seam under the double pressure relief coefficient β is established, as shown in Formula 11.

$$\begin{cases} B_0 = 8.125 \ln r + 64.287 \\ B_{0.5} = 8.1371 \ln r + 68.391 \\ B_{1.0} = 7.6406 \ln r + 64.274 \\ B_{1.5} = 8.5924 \ln r + 64.266 \end{cases} \qquad (11)$$

In Formula 11, B_0, $B_{0.5}$, $B_{1.0}$, and $B_{1.5}$, are the microscopic pore volume proportions, %, before and after the test of vertical slot coal seam and β = 0.5, 1.0 and 1.5, respectively; r is the microscopic pore size, μm.

The above mathematical model can design, predict and control the pore distribution of vertical slot coal seam, so as to improve the permeability of coal seam, the effect of pumping and the effect of preventing outburst.

5 Discussion

5.1 Innovative achievements

The paper found the double pressure relief effect of hydraulic slit + gas extraction on vertical slot coal seam, put forward the double pressure relief coefficient, revealed the evolution law of macro - fine - micro structure of vertical slot coal seam under the double pressure relief effect, and built the mathematical model of double pressure relief coefficient and pore fracture parameter evolution. The mathematical model can quantitatively design, predict and control the spatial distribution of macroscopic fractures, microscopic fractures and pores, and provide theoretical basis for stress and gas dual pressure relief and permeability enhancement, gas extraction and coal and gas outburst prevention.

Compared with the existing research, this study proposed the use of double pressure relief coefficient for the first time. The macro - fine - micro law and mathematical model of vertical slot coal seam

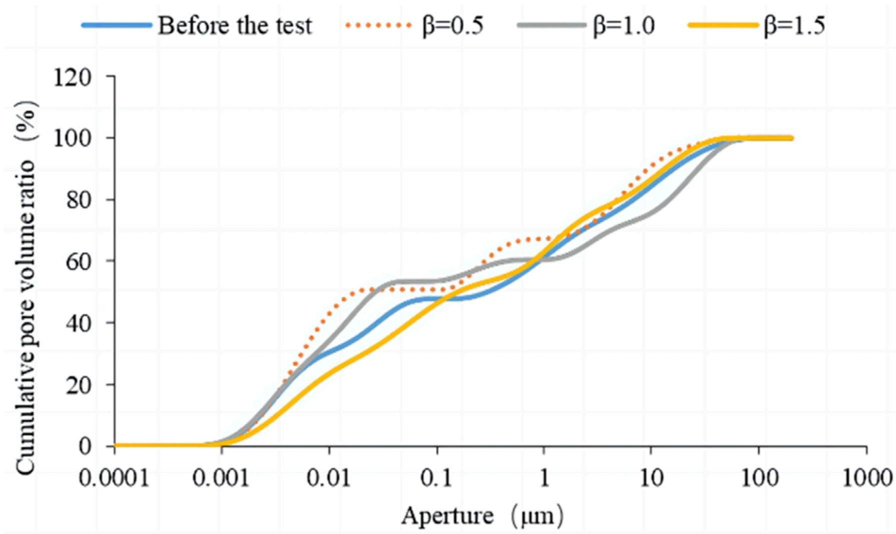

FIGURE 14
Cumulative volume proportion of pores with different pore sizes.

under the stress and gas relief are studied quantitatively. The research results also laid a certain theoretical foundation for the formation of a new method of double pressure relief in deep coal seams for accurate and efficient outburst prevention.

Of course, this paper only studies the pore fracture evolution law and mathematical model of vertical fractured coal seam under the paths of double pressure relief coefficient β = 0.5, 1.0 and 1.5. In the next step, more research should be carried out on the evolution law and mathematical model of vertical fractured coal seam of the double pressure relief coefficient.

5.2 The implications for field-scale applications

(1) The proposal of the double pressure relief coefficient can predict, design and control the mechanical strength of the coal body in the seam, so that the strength of the coal seam after pressure relief meets the requirements of outburst prevention. It can not only fully relieve the *in situ* stress of the coal seam, but also avoid excessive damage to the strength of the coal seam.
(2) The proposal of the dual pressure relief coefficient can predict, design and control the macroscopic, mesoscopic and microscopic fractures of the coal body in the seam slot, as well as rationally arrange the macroscopic, mesoscopic and microscopic fracture network, so as to fully relieve the pressure and enhance the permeability of the coal seam, and achieve efficient mining and outburst prevention of the coal seam.

5.3 The challenges in upscaling lab-scale β to *in situ* conditions

(1) The relevant research on the double pressure reduction coefficient in the laboratory, it simplifies the model. The *in situ* conditions also need to take into account the influences of factors such as the coal seam dip angle, coal seam thickness, hardness, and burial depth changes.
(2) Under *in situ* conditions, the slot coal is also affected by water. In the next step, it is necessary to conduct research on the dual pressure relief and outburst prevention mechanism of the slot coal under the multi-field coupling effect of water, stress and gas.
(3) Under *in situ* conditions, the stress of coal seams is mostly in a triaxial unequal pressure state, which has certain deviation compared with the laboratory research. The next step should be to carry out the research under the triaxial unequal pressure state.

5.4 The dual pressure relief coefficient inform dynamic models of gas outburst

The double pressure relief coefficient can provide information for the dynamic model of gas outburst. There are mainly the following three aspects.

(1) It is well known that coal and gas outbursts mainly occur in coal roadways. The proposal of the double pressure relief coefficient can analyze the strength of the coal in the front of the coal roadway and reveal the macroscopic mechanical failure mechanism of the coal in the coal roadway. Not only can the influence of adsorbed gas and free gas on the strength of slotted coal body be analyzed, but also the mechanism of the mechanical failure of gas on slotted coal can be revealed.
(2) The experiments show that after the dual pressure relief effects of hydraulic cutting and gas extraction of the coal in front of the coal roadway, the peak stress of the coal in front of the coal roadway transfers to the deep part of the coal roadway. The proposal of the double pressure relief coefficient not only calculates the peak stress reduction value and the

increase value of the peak position of the coal in the front of the coal roadway before and after double pressure relief, but also can obtain the main factors for the stress pressure relief regulation of the coal in the seam groove at the front of the coal roadway excavation. Thus, the dual pressure relief mechanism of coal stress and gas in front of the coal roadway is obtained.

(3) The proposal of the double pressure relief coefficient can not only construct the mechanical-energy model of the coal in the front seam groove of the coal roadway, determine the quantitative relationship between the double pressure relief coefficient of the coal in the seam groove and the strength of the coal, but also use the double pressure relief coefficient as an intermediate variable to deduce the dual index criterion of force-energy for coal roadway outburst prevention.

In conclusion, the proposal of the double pressure relief coefficient can provide the possibility for quantitatively revealing the mechanical failure mechanism, the double pressure relief mechanism of stress and gas, and the double pressure relief outburst prevention mechanism of the coal in the front seam groove of the coal roadway from the perspectives of mechanical strength, double pressure relief of stress and gas, and energy evolution.

6 Conclusion

By carrying out mechanical seepage experiments of vertical slot coal samples under different double pressure relief coefficients, the evolution law and mathematical model of pore fracture are obtained. The main conclusions are as follows.

(1) Experimental results show that with the increase of double pressure relief coefficient β, the fracture of vertical slot coal seam gradually weakens, and the failure range decreases from tension failure to split failure. It provides a theoretical basis for the scientific placement of slot number, hole spacing and hole sealing depth.

(2) The experiment shows that the macro-fracture of seam plays a leading role. When $\beta = 1.0$ ($\triangle\sigma = \triangle P$), the macroscopic fracture is the most developed. When $\beta = 0.5$ ($\triangle\sigma = 0.5\triangle P$), the meso-fracture is the most developed. It provides a scientific basis for the reasonable arrangement of macroscopic and microscopic fracture network to improve the permeability of coal seam.

(3) The results show that the proportion of micro pores and small pores before and after test the vertical slot coal seam is the largest, followed by the proportion of large pores, and the proportion of middle pores is the smallest. The cumulative fracture volume increases gradually and the growth rate is similar after the test. The microscopic mechanism of coal permeability increase under double pressure relief is revealed.

(4) It is found that there is a quadratic or cubic functional relationship between the fracture parameters of the vertical slot coal seam and the double pressure relief coefficient β. It is found that there is a logarithmic function relationship between pore size and cumulative volume ratio. It provides a scientific basis for quantitative design, prediction and control of coal seam gas permeability, pumping effect and outburst prevention effect

Data availability statement

The original contributions presented in the study are included in the article/supplementary material, further inquiries can be directed to the corresponding author.

Author contributions

ZW: Conceptualization, Formal Analysis, Funding acquisition, Investigation, Writing – original draft. ZG: Methodology, Supervision, Writing – review and editing. DS: Data curation, Resources, Writing – review and editing. YZ: Supervision, Writing – review and editing, Data curation. HY: Data curation, Resources, Writing – original draft.

Funding

The author(s) declare that financial support was received for the research and/or publication of this article. This work is supported by Chongqing Natural Science Foundation Project (CSTB2022NSCQ-MSX0276, cstc2021jcyj-msxmX1149, CSTB2022NSCQ-MSX0373), National Natural Science Foundation of China Surface Project (52,274,246, 52,474,277), and Technological Innovation and Entrepreneurship Fund Special Project of Tiandi Technology Co., Ltd. (2021-2-TD-ZD008).

Conflict of interest

The authors declare that the research was conducted in the absence of any commercial or financial relationships that could be construed as a potential conflict of interest.

The authors declare that this study received funding from Tiandi Technology Co., Ltd. The funder had the following involvement in the study: data collection.

Generative AI statement

The authors declare that no Generative AI was used in the creation of this manuscript.

Publisher’s note

References

Agi, B., Joan, S., and Suzanne, D. (2014). Horizontal stress anisotropy and effective stress as regulator of coal seam gas zonation in the Sydney Basin, Australia. *Int. J. Coal Geol.* 132 (1), 103–116. doi:10.1016/j.coal.2014.08.008

Barbara, B. (2021). Effect of the depth of impact hazard on the adsorption capacity of coal. *Fuel* 306 (1), 121611. doi:10.1016/j.fuel.2021.121611

Chen, S. D., Tang, D. Z., Su, T., Xu, H., Song, L., Zhao, J. L., et al. (2017). *In-situ* stress measurements and stress distribution characteristics of coal reservoirs in major coalfields in China: implication for coalbed methane (CBM) development. *Int. J. Coal Geol.* 182, 66–84. doi:10.1016/j.coal.2017.09.009

Cheng, X., Zhao, G. M., Li, Y. M., Meng, X. R., and Tu, Q. Y. (2020). Key technologies and engineering practices for soft-rock protective seam mining. *Int. J. Min. Sci. Technol.* 30 (06), 889–899. doi:10.1016/j.ijmst.2020.07.006

Cheng, X. Y., Zhang, Q. H., Zhang, Z. G., Zou, Y. L., and Guo, J. J. (2021). Stress relief and stimulation of coal reservoir by hydraulic slotting. *Adv. Civ. Eng.* 2021, 6664696. doi:10.1155/2021/6664696

Dang, J. X., Tu, M., Zhang, X. Y., and Pu, Q. W. (2021). Analysis of the influence of upper protective layer mining on the effect of pressure relief and protection of coal and rock masses between the lower overburden layers. *Hindawi Ltd.* 2021, 1–8. doi:10.1155/2021/8682156

Du, J. L. (2023). Research and application of high-pressure hydraulic slot anti-reflection technology for low-permeability outburst coal seams. *Wuhan Univ. Eng.* doi:10.27727/d.cnki.gwhxc.2022.000354

Fan, S. X. (2021). Study on the mechanism of fractures propagation and permeability enhancements induced by liquid CO_2 fracturing. *Chin. J. Rock Mech. Eng.* 40 (8), 1728. doi:10.13722/j.cnki.jrme.2021.0442

Fan, S. X., Wen, H., Jin, Y. F., Chen, J., Tong, X. Z., Cheng, X. J., et al. (2021). Initiation pressure model for liquid CO_2 fracturing through upward penetrating boreholes and its engineering verification. *Chin. J. Rock Mech. Eng.* 40 (4), 703–712. doi:10.13722/j.cnki.jrme.2020.0228

Guo, J. J., Li, W., Yang, J., and Wang, Y. (2021). A discrete numerical simulation of micromechanics for dense coal granular systems: implication for coal and gas outbursts. *Powder Technol.* 392, 448–458. doi:10.1016/j.powtec.2021.07.032

Han, J. (2022). *Evolution mechanism of the coupling between reservoir water effective stress and permeability during coalbed methane production: a case study of the 3# coal seam in the Sihe Mine in the southern Qinshui area*. China University of Mining and Technology. doi:10.27623/d.cnki.gzkyu.2022.002772

He, A. P., Fu, H., Huo, B. J., and Fan, C. J. (2020). Permeability enhancement of coal seam by lower protective layer mining for gas outburst prevention. *Shock Vib.* 2020 (5), 1–12. doi:10.1155/2020/8878873

Hu, N. (2021). *Deep high ground stress Analysis of damage mechanism and stability of surrounding rock in stopes under certain conditions[D]*. University of Science and Technology Beijing. doi:10.26945/d.cnki.gbjku.2021.000224

Jia, H. Y. (2022). *Protected at different distances Research on the evolution law and application of layer mining unloading permeability*. Beijing: China University of Mining and Technology. doi:10.27624/d.cnki.gzkbu.2020.000066

Kang, H. P., Gao, F. Q., Xu, G., and Ren, H. W. (2023). Mechanical behaviors of coal measures and ground control technologies for China's deep coal mines – a review. *Chin. J. Rock Mech. Geotechnical Eng. Engl.* 15 (1), 37–65. doi:10.1016/j.jrmge.2022.11.004

Kenyon, W. E. (1992). Nuclear magnetic resonance as a petrophysical measurement. *Nucl. Geophys.* 6 (2), 153–171.

Kleinberg, R. L., Kenyon, W. E., and Mitra, P. P. (1994). Mechanism of NMR relaxation of fluids in rock. *J. Magnetic Reson. Ser. A* 108 (2), 206–214. doi:10.1006/jmra.1994.1112

Li, J. G. (2019). Stress transfer technology for pre-excavation tunnels in close coal seams. *Coal Mine Saf.* 50 (04), 90–94. doi:10.13347/j.cnki.mkaq.2019.04.021

Li, L. J., Liu, D. M., Cai, Y. D., Wang, Y. J., and Jia, Q. F. (2021). Coal structure and its implications for coalbed methane exploitation: a review. *Energy Fuels* 35 (1), 86–110. doi:10.1021/acs.energyfuels.0c03309

Li, Q. (2021). *Mechanism and experimental research on the anti-reflection mechanism and application of jet slit composite fracturing in coal mines*. Chongqing University. doi:10.27670/d.cnki.gcqdu.2019.003350

Li, S. G. (2023). Fractures caused by high-pressure air blasting in low-permeability coal seams research and application of anti-reflection technology. *Liaoning Univ. Eng. Technol.* doi:10.27210/d.cnki.glnju.2018.000040

Liu, T., Lin, B., and Zou, Q. (2015). Pore structure change characteristics of coal after pre-pumping with slit in Yangliu Coal Mine. *Nat. gas earth Sci.* 26 (10), 10. CNKI:SUNTDKX.0.2015-10-024.

Pang, L. L. (2021). Gas permeability characteristics and disaster-causing mechanisms of and quot, three soft and quot, coal seams. *Henan Univ. Sci. Technol.* doi:10.27116/d.cnki.gjzgc.2019.000320

Pang, L. N., Fu, S. J., and Su, B. (2021). Research and application of anti-scour mechanism of large-diameter coal seam drilling and roof pre-split holes. *Coal Mine Saf.* 52 (09), 183–189. doi:10.13347/j.cnki.mkaq.2021.09.030

Qin, H. J., Wei, J. P., Li, D. H., and Wu, Z. Q. (2021). Research on the mechanism of in situstress in the process of coal and gas outburst. *J. China Univ. Min. and, Technol.* 50 (5), 933–942. doi:10.13247/j.cnki.jcumt.001327

Ren, P. L., Liu, Y. W., Han, H. K., Wang, D., Zuo, W. Q., Li, Y. Q., et al. (2022). A review on prediction and early warning Study on influence laws of coal flushing rate on coal seam stress relief and gas extraction. *Coal Sci. Technol.* 50 (10), 102–109. doi:10.13199/j.cnki.cst.ZGCS-012

Ren, W. (2022). *Multi-scale fractal of deep coal body pore and fracture structure Research on characterization and permeability mechanism*. Beijing: China University of Mining and Technology. doi:10.27624/d.cnki.gzkbu.2022.000077

Rong, T. L. (2020). *Deep coal bodies Research on the evolution law of permeability under the action of multi-field coupling*. Beijing: China University of Mining and Technology. doi:10.27624/d.cnki.gzkbu.2019.000103

Shi, Z. S. (2023). Pressure relief effect of upper protective layer mining thickness and mechanism research. *Liaoning Univ. Eng. Technol.* doi:10.27210/d.cnki.glnju.2018.000025

Shu, L. Y. (2020). Key structures causing disasters in coal and gas outbursts Mechanism. *China Univ. Min. Technol.* doi:10.27624/d.cnki.gzkbu.2019.000138

Su, E. L. (2022). *Structural response of bituminous coal under the action of supercritical CO_2 and its influence mechanism on mechanical and permeability properties*. Chongqing University. doi:10.27670/d.cnki.gcqdu.2021.000362

Su, H., Zhao, Y. C., Liu, J. C., Wang, M., and Zhang, X. W. (2015). Research on the influence of the position and size of the pressure relief tunnel on the bottom drum of the lower tunnel. *Coal Technol.* 34 (02), 53–55. doi:10.13301/j.cnki.ct.2015.02.020

Sun, S. Q., Zhang, Q., Yan, Z. M., Zhang, J., Wang, Y. W., and Zheng, K. G. (2017). Practice of permeability enhancement through overal hydraulic fracturing of long hole inoutburst prone solt crushed coal seam with low permeability. *Joumal china Coal Soc.* 42 (9), 2337–2344. doi:10.13225/j.cnki.jccs.2017.0689

Tu, Q. Y., and Cheng, Y. P. (2019). Stress evolution and coal seam deformation through the mining of a remote upper protective layer. *Energy sources.* 41 (1-6), 1–11. doi:10.1080/15567036.2018.1518352

Wang, F. T., Ren, T., Tu, S. T., Frank, H., and Naj, A. (2012). Implementation of underground longhole directional drilling technology for greenhouse gas mitigation in Chinese coal mines. *Int. J. Greenh. Gas Contro* 11, 290–303. doi:10.1016/j.ijggc.2012.09.006

Wang, N., and Li, S. G. (2022). Study on coal mechanical damage law and anti-refection effects under fracturing fluid corrosion affecting. *Coal Sci. Technol.* 50 (5), 150–156. doi:10.13199/j.cnki.cst.2022-0209

Wang, X. (2022). *Research on damage behavior and permeability characteristics of deep coal bodies*. Beijing: China University of Mining and Technology. doi:10.27624/d.cnki.gzkbu.2022.000089

Wei, J., Liu, S. X., Yang, R. S., Lai, W. J., and Xue, W. P. (2022). Mechanism of aging deformation zoning of surrounding rock in deep high stress soft rock roadway based on rock creep characteristics. *J. Appl. Geophys.*, 202. doi:10.1016/j.jappgeo.2022.104632

Xue, J. H., Xiao, J., Du, X. H., and Shi, Y. (2023b). Current status and development trends of pressure relief gas extraction in coal mine protective layer mining in my country. *Coalf. Geol. Explor.* 51 (06), 50–61. doi:10.12363/issn.1001-1986.22.11.0894

Xue, S., Tu, Q. Y., Yuan, W. H., Yang, Y., Zhao, Z. H., and Li, X. Y. (2023a). Occurrence and development criteria of coal and gas outbursts based on energy conversion. *Fuel* 341, 127781. doi:10.1016/j.fuel.2023.127781

Yang, D. D., Chen, Y. J., Tang, J., and Jiang, C. L. (2021). Comparative experimental study of methods to predict outburst risk when uncovering coal in crosscuts. *Fuel* 288, 119851. doi:10.1016/j.fuel.2020.119851

Yang, Z. L. (2023). *High-stress soft rock tunnel bottom in Shendong Mining Area Research on mechanism and control technology*. Beijing: China University of Mining and Technology. doi:10.27624/d.cnki.gzkbu.2021.000135

Yao, Y. B., and Liu, D. M. (2016). Petrophysics and fluid properties characterizations of coalbed methane reservoir by using NMR relaxation time analysis. *Coal Sci. Technol.* 44 (6), 14–22. doi:10.13199/j.cnki.cst.2016.06.003

Ying, C., Fan, B., and Qin, Q. (2020). Liquid CO_2 phase transition fracturing technology and its application in enhancing gas drainage of coal mines. *Adsorpt. Sci. and Technol.* 38 (9a10). doi:10.1177/02636174209525

Yuan, L. (2021). Research progress of mining response and disaster prevention and control in deep coal mines. *J. China Coal Soc.* 46 (3), 716–725. doi:10.13225/j.cnki.jccs.YT21.0158

Yuan, L., Wang, E. Y., Ma, Y. K., Liu, Y. B., and Li, X. L. (2023a). Research progress of coal and rock dynamic disasters and scientific and technological problems in China. *J. China Coal Soc.* 48 (5), 1825–1845. doi:10.13225/j.cnki.jccs.2023.0264

Yuan, L., Wu, J. S., and Yang, K. (2023b). Safe intelligent precise coal mining key technology and application. *J. Min. Saf. Eng.* 40 (5), 861–868. doi:10.13545/j.cnki.jmse.2023.0240

Yue, L. J. (2022). Research and application of high-pressure hydraulic slotted drainage technology in Pingdingshan No. 10 Mine. *Liaoning Univ. Eng. Technol.* doi:10.27210/d.cnki.glnju.2021.000124

Zhai, C., Sun, Y., Fan, Y. R., Yang, P. Q., Ge, X. M., and Wu, F. (2022). Application and prospect of low-field nuclear magnetic resonance technology in accurate characterization of coal pore structure. *J. China Coal Soc.* 47 (2), 828–848. doi:10.13225/i.cnki.jccs.XR21.1766

Zhai, W., Guo, Y. C., Ma, X. C., Li, N. L., Zhang, P., Ma, K., et al. (2021). Research on hydraulic fracturing pressure relief technology in the deep high-stress roadway for surrounding rock control. *Adv. Civ. Eng.* 2021. doi:10.1155/2021/1217895

Zhang, H. (2021). *Structural coal seam excavation working face regional bedding hydraulic caving enhanced gas drainage mechanism and engineering application*. China University of Mining and Technology. doi:10.27623/d.cnki.gzkyu.2020.000536

Zhang, J. G. (2020). Study on key technologies of collaborative mining in deep coal seam with high gas and low permeability. *Coal Sci. Technol.* 48 (9), 66–74. doi:10.13199/j.cnki.cst.2020.09.007

Zhang, M. J., Li, Y. X., Yan, J. W., Tan, Z. H., and Liu, K. X. (2022). Determination of influence radius of hydraulic punch extraction by gas emission attenuation characteristic method. *Coal Seience Technol.* 50 (7), 156–162. doi:10.13199/j.cnki.cst.2020-1049

Zhang, R., Cheng, Y. P., Yuan, L., Zhou, H. X., Wang, L., and Zhao, W. (2019). Enhancement of gas drainage efficiency in a special thick coal seam through hydraulic flushing. *Int. J. Rock Mech. Min. Sci.* 124, 104085. doi:10.1016/j.ijrmms.2019.104085

Zhang, Y. J., Huang, Z. F., and Li, C. C. (2018). High-pressure water jet annular cutting joint self-relief mechanism and application. *J. Coal Sci. Technol.* 43 (11), 3016–3022. doi:10.13225/j.cnki.jccs.2018.8014

Zhang, Y. J., Zou, Q. L., Yang, H. M., Chen, Z. H., Cao, J. J., and Cheng, Z. H. (2023). Outburst prevention mode and key technology of joint drainage of upper and lower wells in outburst coal seam groups. *J. Coal Sci.* 48 (10), 3713–3730. doi:10.13225/j.cnki.jccs.s022.1663

Zhao, B. (2022). *Experimental study on stress-driven coal and gas outburst simulation[D]*. Chongqing University. doi:10.27670/d.cnki.gcqdu.2020.000416

Zhao, Y. P., and Zhang, M. B. (2020). "Research and application of hydraulic punching antireflection technology for rock cross-cut coal uncovering in deep outburst coal seam[C]," in *2020 international conference on urban engineering and management science (ICUEMS)*. doi:10.1109/ICUEMS50872.2020.00124

Zheng, J. W., Ge, Z. L., Lu, Y. Y., Zhou, Z., Zhou, J., and Fu, W. Y. (2023). Prediction of fracture initiation pressure for slotting-directional hydraulic fracturing based on the anisotropy of coal. *J. Energy Resour. Technology-Transactions Asme* 145 (11). doi:10.1115/1.4062960

Zou, Q., Lin, B., Zhu, C., Liu, T., Zhou, Y., Yan, F., et al. (2014b). Variation in the pore structure of coal after hydraulic slotting and gas drainage. *Adsorpt. Sci. and Technol.* 32 (8), 647–666. (in Chinese). doi:10.1260/0263-6174.32.8.647

Zou, Q. L., Lin, B. Q., Liu, T., Zhu, C. J., Yan, F. Z., and Zhou, Y. (2014a). Variation of gas adsorption of coal after hydraulic slotting and pre-draining. *J. rock Mech. Eng.* 33 (010), 2117–2124. doi:10.13722/j.cnki.jrme.2014.10.019

Zou, Q. L., Liu, H., Jiang, Z. B., and Wu, X. A. (2021). Gas flow laws in coal subjected to hydraulic slotting and a prediction model for its permeability-enhancing effect. *Energy Sources Part A Recovery Util. Environ. Eff.* 2021 (7), 8628–8642. doi:10.1080/15567036.2021.1936692